Available online at www.sciencedirect.com

ScienceDirect

ELSEVIER

Polymer Degradation and Stability 93 (2008) 1008–1023

Polymer Degradation and Stability

www.elsevier.com/locate/polydegstab

A new approach on the thermal stability of SDS copolymer for HMPSA, Part I: Oxidation kinetics for the whole process

Junying Zhang [a,b,*], Young-Jun Park [a], Hyun-Joong Kim [a,*]

[a] *Laboratory of Adhesion and Bio-Composites, Program in Environmental Materials Science, Seoul National University, Seoul 151-921, Republic of Korea*
[b] *Laboratory of Adhesives and Polymerization Technology, Beijing University of Chemical Technology, Beijing 100029, PR China*

Received 4 November 2007; accepted 29 December 2007
Available online 12 January 2008

Abstract

The poor aging property of the styrene–diene–styrene (SDS) triblock elastomer copolymer hot-melt pressure-sensitive adhesives (HMPSAs) has raised the importance of research on the aging and anti-aging properties of SDS triblock copolymers, such as styrene–butadiene–styrene (SBS) and styrene–isoprene–styrene (SIS). A mechanistic scheme based on the standard scheme for radical chain oxidation, but taking into account the decomposition of the oxidation-induced peroxide, was built. The kinetic equation of oxygen uptake was deduced from the proposed mechanism, which is composed of a set of reasonable parameters. The relationships among the parameters to induction time, maximum oxygen uptake and the maximum oxidation rate were examined. Numerical simulation methods were established to obtain parameters from the experiment data, by which most kinetic equations of oxygen uptake of the ingredients for HMPSAs were numerically fitted and the relativity of the model to the data was discussed. The study results should prove useful for future studies on the anti-aging performance of other materials.

Keywords: Thermal stability; Oxidation; Simulation; SBS; SIS; HMPSAs

1. Introduction

The structure and properties of styrene–diene–styrene (SDS) triblock copolymers, such as styrene–butadiene–styrene (SBS) and styrene–isoprene–styrene (SIS), are nearly ideal for inclusion in PSA formulations, since they combine high cohesive strength and good processability, and can be readily tackified [1]. These block copolymers constitute the major component in a variety of commercial PSAs, but their tendency toward aging changes is not fully understood even now. This aging is usually manifested in the loss of tackiness and cohesive strength, and it is reasonable that some of these changes may be related to the unsaturation that exists in the diene midblocks [2]. The thermo-oxidation of the SDS polymer causes scissions and crosskicking [3–5] which deteriorates PSA during the operation. The double bond present in the diene part of the elastomer is more susceptible to thermal and oxidative degradation. Saturation of the polymer backbones significantly improves the resistance to degradation [6]. Hydrogenation of diene elastomers is an excellent example of chemical modification which improves both the anti-aging and physical properties of an existing elastomer, but it increases the price and lowers the PSA properties. The most effective approach for improving the long term performance and anti-thermo-oxidation ability is to compound some antioxidant. The practical requirements for the improvement of polymer durability have stimulated academic research on the stabilization efficiency of various large categories of antioxidants. Starting from commercial products such as sterically hindered phenols or amines, many compounds have attracted interest.

Most oxidation mechanisms of plastics and elastomers, and stabilization mechanisms of antioxidants have been proposed and reviewed [7–14]. Much work has been carried out on

---

* Corresponding authors. Laboratory of Adhesion and Bio-Composites, Program in Environmental Materials Science, Seoul National University, Seoul 151-921, Republic of Korea.

E-mail addresses: zjybuct@gmail.com (J.Y. Zhang), hjokim@snu.ac.kr (H.-J. Kim).

0141-3910/$ - see front matter © 2008 Elsevier Ltd. All rights reserved.
doi:10.1016/j.polymdegradstab.2007.12.016

the thermal oxidation of polyolefins. However, only a few thermo-oxidative studies of SDS-based hot-melt pressure-sensitive adhesives (HMPSAs) and their effect on performance have been reported [15,16].

The oxidation aging phenomena are very complex physical and chemical processes with too many variables for the real aging rate to be expressed using simple models and variables. The correct variables include the service temperature, impurity, structure and morphology, antioxidant, thickness, oxygen pressure and load stress, etc. With a special model and under definite conditions, much experimental research has been conducted on the kinetics of change in the various polymer properties upon thermo-oxidative aging [17,18].

A detailed explanation of the ‘‘critical antioxidant concentration’’ and the related concept of minimal antioxidant concentration was elaborated by Gugumus [19–21], and the consequent kinetics were deduced to predict the lifetime of the inhibition system featuring strong deviations from the predicted data in the lower part of the concentration range. Both the ‘‘critical antioxidant concentration’’ and or the ‘‘minimal antioxidant concentration’’ methods are very restricted; the oxidation level method seems to be generally applicable.

The amount of absorbed oxygen per unit mass of the polymer material is the most often measured on thermo-oxidative degradation. Analysis of the experimental data of oxygen uptake as a measure of the thermo-oxidative degradation of different polymers, in both open and closed systems, presents three main types of kinetic curve, as illustrated in Fig. 1. The related kinetics expression was given by Emanue [9].

The first curves (Fig. 1(a)) of the self-accelerated type with a distinct induction period are described by the following equation:

$$N_{O_2} = a(t - t_0)^2 \tag{1}$$

where N_{O_2} is the number of moles of oxygen taken up by the polymer, ‘‘a’’ is a constant, and ‘‘t_0’’ is the time starting from the process occurs in the regime of auto-oxidation. Eq. (1) can only be used in a constricted stage during auto-oxidation because it is actually unacceptable at the initial period of time from 0 to t_0, in which N_{O_2} gradually decreases to zero, which disagrees with the incremental nature of the oxygen uptake. The other limitation of the equation is the absence of any oxidation slowdown during the last stage of oxidation. Therefore, the parameters ‘‘a’’ and ‘‘t_0’’ are not useful in explaining the oxidation.

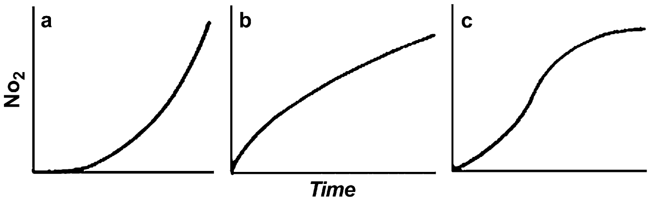

Fig. 1. Main types of kinetic curve of oxygen uptake on thermo-oxidative aging of polymers.

Curves of the second type, as shown in Fig. 1(b), are described by the following equation:

$$N_{O_2} = N_{O_2}^{\infty}\left(1 - e^{-kt}\right) \tag{2}$$

where $N_{O_2}^{\infty}$ is the limiting amount of oxygen capable of being absorbed during oxidation and k is the effective rate constant of oxidation. This equation cannot explain the induction time of either the inhibition or un-inhibition system at low temperature because it is merely a mathematic equation to simulate the shape of the curve.

Curves of the third type (the most common type of kinetic curve), as shown in Fig. 1(b), are described by the following equation:

$$N_{O_2} = N_{O_2}^{\infty}\frac{1 - e^{-kt}}{1 + be^{-\beta kt}} \tag{3}$$

where β and b are constants depending on the polymer structure and temperature, respectively. It is reported that such kinetic curves are essentially characteristic of the oxidation of hetero-chain polymers at 250–400 °C. Oxidation of polymers at the initial stage proceeds under self-acceleration, whereas the rate of oxidation at high degrees of oxidation drops owing to the burning up of the reactive groups. The experimental points satisfactorily fit the theoretical curve described by Eq. (3) for parameter values of $\beta = 6$ and $b = 5$ (Fig. 1(c)). However, the method for the deduction of this equation has not been elucidated, and the physical meaning of the parameters b, β and k has not been reported.

It has been recognized that many oxidation reactions are chain reactions. Due to the difficulty in discerning different free radicals and measuring their amount, the basic theory of oxidation chain reactions was deduced based on the hypothesis of the existence of a steady or stationary state for the reactive entities, such as atoms and free radicals, present in a system. In other words, the rate of formation of the short-lived intermediates is equal to their rate of disappearance in a stationary state during which the overall reaction does not advance to any significant amount. The disappearance rate of the reactive entities includes the bimolecular termination between two free radicals, as well as the nature of the inhibition reactions by antioxidants.

An outline can be formed for which a true understanding of any aging mechanism and the relationship between the degree of oxidation and the performance is difficult to achieve quantitatively from the applicant point of view. The most practical method is to select a high efficiency antioxidant by artificial aging methods based on a simple model. At best, we can describe it qualitatively and measure some systematic dependencies. The modest aim of this article is to find a simple practical method to simulate the oxygen uptake curves under aging with various antioxidants, without requiring a full understanding of the problem. It is hoped that these efforts will yield some useful results to form the basis for future research.

2. Theoretical and methods

2.1. The mechanism of autoxidation

The autoxidation process can usually be described as a series of chain reactions [19,22,23] including initiation, propagation and termination processes. A 17-step, pseudo-detailed mechanism was proposed by Zabarnick [22] to represent the dominant chemical kinetics of jet fuel thermal oxidation chemistry, and was further developed into a 19-step model by him and his coworkers Kuprowicza et al. [23]. Table 1 lists the reactions and rate constants. The fuel is modeled as a single species, RH, which is assumed to have the chemical properties of a straight-chain alkane. Reactions 1 through 4, together with reaction 10, correspond to a simplified autoxidation chain. The chemistry associated with peroxide-radical-inhibiting antioxidant molecule (AH) is represented by reactions 5 through 9. The unimolecular decomposition of hydroperoxides (RO_2H) is represented by reaction 11, and the related free radical chemistry associated with this decomposition is represented by reactions 12 through 16. Finally, the chemistry associated with a peroxide decomposer species (SH) is represented by reaction 17.

The alkyl free radical reacts very easily and quickly with abundant oxygen in the test state to form peroxyl free radical so that the most terminated reaction takes place on the two peroxyl free radicals.

Most of the studies have presented exhaustive mechanisms [17,19,24–26] with schemes comprising far too many elementary steps, some of which may not be as important as others from theoretical and kinetic considerations. Any kinetic analysis involving all of these reactions would of necessity be very complicated with unwieldy parameter estimation. On the other hand, the importance of certain key chain transfer and termination reactions seems to have been lost following their relegation to secondary side reaction steps. In this work, we therefore propose to create a reaction network which is both compact and more consistent, by using the available and pertinent information in the literature, as shown in Table 2.

2.2. The kinetics of oxygen uptake

A careful study of the previous works on the kinetic modeling of polymer autoxidation reveals that the elementary reactions are too complicated for their interrelationships to be understood due to the very high activity of the free radicals and the difficulty in measuring and determining their concentration. The rate constant can only be roughly predicated. However, the consumption of the oxygen volume during the oxidation process can easily and accurately be measured using the equipment illustrated in Fig. 1. The key to polymer antioxidation is the selection of a high efficiency antioxidant to minimize the effect of oxidation and to extend the service time of the materials. The oxygen uptake curve illustrates some aspects of the oxidation behavior, such as the induced time, oxidation rate and the amount of oxygen consumed. Further questions include the relations between the elementary reaction and the oxygen uptake, and the reason for the presence of so many types of kinetic curve among the oxidization condition. This paper presents an attempt to deduce the oxygen uptake curves by the mechanism of autoxidation.

From the reactions listed in Table 1, it is known that the oxygen consumption rate is equal to the RO_2• forming rate. The oxygenation reaction 2 of R• with O_2 is generally assumed to be a very fast reaction with almost zero activation energy, causing the concentration of R• to be much smaller than that of RO_2•, and hence the termination reaction 10 of two alkyl radicals R• rarely occurs, especially for the macromolecule radical. Due to the abundant oxygen conditions, we can assume that the oxygen consumption rate is equal to the

Table 1
Pseudo-detailed chemical kinetic mechanisms [23]

#	Reaction	(a)		(b)	
		A ($mol^{-1} \cdot L \cdot s^{-1}$)	E_a (kcal/mol)	A ($mol^{-1} \cdot L \cdot s^{-1}$)	E_a (kcal/mol)
1	$I \rightarrow R^\bullet$	1×10^{-3}	0.0	1×10^{-3}	0.0
2	$R^\bullet + O_2 \rightarrow RO_2^\bullet$	3×10^{9}	0.0	3×10^{9}	0.0
3	$RO_2^\bullet + RH \rightarrow RO_2H + R^\bullet$	3×10^{9}	12.0	3×10^{9}	12.0
4	$RO_2^\bullet + RO_2^\bullet \rightarrow$ termination	3×10^{9}	0.0	3×10^{9}	0.0
5	$RO_2^\bullet + AH \rightarrow RO_2H + A^\bullet$	3×10^{9}	5.0	3×10^{9}	5.0
6	$AO_2^\bullet + RH \rightarrow AO_2H + R^\bullet$	3×10^{5}	10.0	3×10^{5}	10.0
7	$A^\bullet + O_2 \rightarrow AO_2^\bullet$	3×10^{9}	0.0	3×10^{9}	0.0
8	$AO_2^\bullet + AH \rightarrow AO_2H + A^\bullet$	3×10^{9}	6.0	3×10^{9}	6.0
9	$AO_2^\bullet + AO_2^\bullet \rightarrow$ products	3×10^{9}	0.0	3×10^{9}	0.0
10	$R^\bullet + R^\bullet \rightarrow R_2$	3×10^{9}	0.0	3×10^{9}	0.0
11	$RO_2H \rightarrow RO^\bullet + {}^\bullet OH$	1×10^{15}	42.0	1×10^{15}	39.0
12	$RO^\bullet + RH \rightarrow ROH + R^\bullet$	3×10^{9}	10.0	3×10^{9}	10.0
13	$RO^\bullet \rightarrow R^\bullet_{prime}$ + carbonyl	1×10^{16}	15.0	1×10^{16}	15.0
14	${}^\bullet OH + RH \rightarrow H_2O + R^\bullet$	3×10^{9}	10.0	3×10^{9}	10.0
15	$RO^\bullet + RO^\bullet \rightarrow RO^\bullet$	3×10^{9}	0.0	3×10^{9}	0.0
16	$R^\bullet_{prime} + RH \rightarrow$ alkane $+ R^\bullet$	3×10^{9}	10.0	3×10^{9}	10.0
17	$RO_2H + SH \rightarrow$ products	3×10^{9}	0.0	3×10^{9}	0.0
18	$RO_2^\bullet \rightarrow R^\bullet + O_2$	N/A	N/A	1×10^{16}	19.0
19	$RO_2^\bullet + R^\bullet \rightarrow$ termination	N/A	N/A	3×10^{9}	0.0

Table 2
Kinetic mechanism related to oxygen uptake

Name of the reaction	No.	Reaction expression	Kinetic equation
Initial reaction of alkyl free radical	1	$R{-}H + O_2 \xrightarrow{k_i} R\bullet + HO_2\bullet(2HO_2\bullet \rightarrow O_2 + H_2O_2 \rightarrow H_2O + 1/2O_2)$	$r_i = k_i[RH][O_2]$ [17]
	2	$R{-}H + M^{III} \xrightarrow{k_i} R\bullet + H^+ + M^{II}(M^{II} + O_2 \xrightarrow{k_i} M^{III})$	$r_i = k_i[RH][M]$
	3	$R{-}H \xrightarrow{k_i} R\bullet$	$r_i = k_i[RH]$
Oxygen uptake reaction	4	$R\bullet + O_2 \xrightarrow{k_o} ROO\bullet$	$r_{O_2} = dN_{O_2}/dt = k_O[R\bullet][O_2]$
The generation of alkyl free radical by chain reaction	5	$R{-}H + ROO\bullet \xrightarrow{k_p} ROOH + R\bullet$	$r_p = k_p\{[ROO^\bullet] + [RO^\bullet] + [HO^\bullet]\}RH = k_p[RX^\bullet][RH]$
	6	$R{-}H + RO\bullet \xrightarrow{k_p} ROH + R\bullet$	
	7	$R{-}H + HO\bullet \xrightarrow{k_p} H_2O + R\bullet$	
Effective terminal reaction	8	$R^\bullet + R^\bullet \rightarrow R{-}R$	Ignore
		$R^\bullet + RO^\bullet \rightarrow R{-}O{-}R$	
		$R^\bullet + HO^\bullet \rightarrow R{-}O{-}H$	
Temporary terminal reaction	9	$ROO^\bullet + ROO^\bullet \rightleftarrows R{-}OOO{-}R \rightarrow O_2 + ROOR$	$r_t = k_t[RX]^2$
	10	$ROO^\bullet + R^\bullet \rightarrow ROOR \rightleftarrows RO^\bullet + RO^\bullet$	
	11	$RO^\bullet + HO^\bullet \rightleftarrows ROOH$	
	12	$RO^\bullet + RO^\bullet \rightleftarrows ROOR$	
Decomposition of peroxide	13	$2ROOH \rightarrow RO^\bullet + RO_2^\bullet + H_2O$	$r_d = k_d[ROOH]_2$

generation rate of alkyl radical R•, resulting in the oxygen uptake kinetic expression being the R• generating kinetic.

The alkyl free radical that is considered to be feasible in autoxidation may be divided into two types: those involving the substrate RH and those involving the decomposition of product ROOH. For the former type, the reaction may be R−H bond breakage under trace metal catalyst or oxygen, as illustrated in Table 2. The decomposition between RH and oxygen to generate radicals has been considered a possible initiation process [22]. For the film specimen in the oxygen-rich autoxidation reaction, the equilibrium oxygen concentration in the sample is constant [25], so the reaction rate is in direct proportion to the RH content, as expressed by the following equation:

$$r_i = k_i[RH] \tag{4}$$

The category of the initiation process involving ROOH can also be divided into two types: those that involve ROOH and ROOR only and those that involve a metal-ion catalyst. In the former type, there are two possible reactions: one (unimolecular) or two (bimolecular) molecular processes. The most likely unimolecular process is the cleavage of the weak bond, as illustrated in reaction 11 of Table 1. Theoretical calculations [27] and experimental data [28] both showed that the activation energy of this process is in the region of 44 kcal, which makes this unimolecular homolysis reaction unattractive as an initiation process. The bimolecular process has been widely held to be an important initiation process, as illustrated as reaction 13 in Table 2.

We mark RX• as the free radical which can react with RH to form R•, for example ROO•, RO• and OH•, and the reaction constants of RX• with RH are almost the same because they have similar activation energy E_a and Arrhenius pre-exponential multiplier value A, which can be seen from Table 1. The generating rate of alkyl free radical by RX• can be expressed by $k_p[RX^\bullet][RH]$. The pseudo kinetic equation of total alkyl free radical is as follows:

$$r_{R\bullet} = k_i[RH] + k_p[RH][RX\bullet] = \big(k_i + k_p[RX\bullet]\big)[RH] \tag{5}$$

The rate of terminal reactions of two RX• is as follows under the assumption of the same termination rate constant.

$$r_t = k_t[RX\bullet]^2 \tag{6}$$

As for the termination of the free radical, theoretically, any two free radicals can easily combine together to stop the ‘‘chain propagation’’ and the terminal reaction rate is proportional to the square of total free radical concentration. However, some terminal products of free radicals are not really the end of free radical. As illustrated in Table 1, the product of two alkoxy free radicals is peroxide (RO_2), which is flexibly decomposed to form two free radicals again. Here, we denote this kind of terminal reaction as a ‘‘Temporary Terminal Reaction’’ (TTR). In other words, the products of TTR function as a store of free radical such as ‘‘a stock of ammunition’’, i.e., this is a new resource for the generation of free radicals to accelerate the oxidation. The main path of disruption of the chain becomes not the reaction between the macroradicals but that of one macroradical with a low molecular weight radical [22], such as, HO•, and hence the terminal products are almost peroxides. The most of free radical termination is TTR reaction and the majority product in the chain reaction is the potential initiator.

The breakdown reaction of the peroxide radical has a high activation energy and, therefore, its role increases with increasing temperature. By the bimolecular process, the decomposition rate is directly proportional to the square of the content of the peroxide group. The following equation can be obtained under the assumption that the decomposition rate constants are similar.

$$r_d = k_d[PO_2]^2 \tag{7}$$

The overall disappearance and generation rates of RX• are equalized by the adjustment of [RX•]. The reactions 5, 6, and 7 in Table 2 do not really eliminate RX• because one RX•

produces one R• then quickly generates a new RX• in the reaction. As the rate of r_i is so small compared to r_d, the equation $r_i + r_\mathrm{d} = r_\mathrm{t}$ can be simplified as:

$$r_\mathrm{d} = r_\mathrm{t} \tag{8}$$

From Eqs. (6)–(8), the relationship between $[\mathrm{PO_2}]$ and $[\mathrm{RX}\bullet]$ can be deduced as shown in the following equation:

$$[\mathrm{PO_2}] = \sqrt{\frac{k_\mathrm{t}}{k_\mathrm{d}}}[\mathrm{RX}\bullet] \tag{9}$$

The oxygen that has been taken up in the oxidizing process, N_{O_2}, is mainly changed to peroxide groups $\mathrm{PO_2}$, RX• and hydroxyl and water, symbolized as the ROH (reactions 6 and 7 in Table 2). Although ROH may be deeply oxidized to form a ketone, carboxylic acid or carbon dioxide, depending on the structure of the substrate RH, this is continuous oxidation beyond the limits of the present assumption and is therefore not considered here. Every consumed molecule of oxygen first formed a peroxyl free radical (reaction 4), most of which were then changed to hydroperoxide (reaction 5). Some of the hydroperoxide decomposed to RO• or HO•, which can react with RH to form the ROH products. We therefore assumed that some of the consumed oxygen has been changed to ROH. If the ratio of oxygen in ROH to the total oxygen N_{O_2} is α, where $[\mathrm{ROH}]/[N_{\mathrm{O}_2}] = \alpha$, and if one mole RX• contains m mole oxygen on average, then the total consumed oxygen N_{O_2} is given by:

$$N_{\mathrm{O}_2} = m[\mathrm{RX}\bullet] + [\mathrm{PO_2}] + \alpha N_{\mathrm{O}_2} = m[\mathrm{RX}\bullet] + \sqrt{\frac{k_\mathrm{t}}{k_\mathrm{d}}}[\mathrm{RX}\bullet] + \alpha N_{\mathrm{O}_2} \tag{10}$$

$$N_{\mathrm{O}_2}(1-\alpha) = [\mathrm{RX}\bullet]\left(m + \sqrt{\frac{k_\mathrm{t}}{k_\mathrm{d}}}\right) \tag{11}$$

$$[\mathrm{RX}\bullet] = \frac{(1-\alpha)N_{\mathrm{O}_2}}{\left(m + \sqrt{\frac{k_\mathrm{t}}{k_\mathrm{d}}}\right)} \tag{12}$$

Eq. (5) can be written as Eq. (13).

$$r_{\mathrm{R}\bullet} = \left(k_i + k_\mathrm{p}\frac{(1-\alpha)N_{\mathrm{O}_2}}{\left(m + \sqrt{\frac{k_\mathrm{t}}{k_\mathrm{d}}}\right)}\right)[\mathrm{RH}] \tag{13}$$

If the initial amount of RH is $[\mathrm{RH}]_0$, every unit of RH consumes $1/n$ unit of oxygen on average, and the oxygen uptake is N_{O_2}, then from $[\mathrm{RH}]_0 - [\mathrm{RH}] = nN_{\mathrm{O}_2}$

$$[\mathrm{RH}] = [\mathrm{RH}]_0 - nN_{\mathrm{O}_2} \tag{14}$$

Let $P = N_{\mathrm{O}_2}$, $A_0 = [\mathrm{RH}]_0$, $A = [\mathrm{RH}]$, Eq. (13) can be expressed as follows:

$$r_{\mathrm{R}\bullet} = \left(k_i + k_\mathrm{p}\frac{(1-\alpha)P}{\left(m + \sqrt{\frac{k_\mathrm{t}}{k_\mathrm{d}}}\right)}\right)(A_0 - nP) \tag{15}$$

The oxygen is consumed in the reaction of alkyl free radical with oxygen, as shown in reaction 4 in Table 2. As this reaction is very fast, and it is difficult for the macroradicals to terminate each other, almost all of the alkyl free radicals react with oxygen, which raises the speed of oxygen uptake up to the generation rate of the alkyl free radical:

$$\frac{\mathrm{d}N_{\mathrm{O}_2}}{\mathrm{d}t} = \frac{\mathrm{d}P}{\mathrm{d}t} = r_{\mathrm{R}\bullet} \tag{16}$$

Let

$$k_2 = \frac{k_\mathrm{p}(1-\alpha)}{m + \sqrt{\frac{k_\mathrm{t}}{k_\mathrm{d}}}} \tag{17}$$

the following differential equation can be deduced from Eqs. (15)–(17).

$$\frac{\mathrm{d}P}{\mathrm{d}t} = (A_0 - nP)(k_i + k_2P) = A_0k_i + (A_0k_2 - nk_i)P - k_2nP^2 \tag{18}$$

$$\frac{\mathrm{d}p}{A_0k_i + (A_0k_2 - nk_i)P - k_2nP^2} = \mathrm{d}t \tag{19}$$

Inspection of the integral table shows that

$$\begin{aligned}\int\frac{1}{ax^2+bx+c}\mathrm{d}x &= -\frac{2}{\sqrt{b^2-4ac}}\ \mathrm{arctanh}\,\frac{2ax+b}{\sqrt{b^2-4ac}}\\ &= \frac{1}{\sqrt{b^2-4ac}}\ln\left|\frac{2ax+b-\sqrt{b^2-4ac}}{2ax+b+\sqrt{b^2-4ac}}\right|\\ &\quad\left(\text{for } 4ac - b^2 < 0\right)\end{aligned} \tag{20}$$

For Eq. (19), $a = -k_2n$; $b = (A_0k_2 - nk_i)$; $c = A_0k_i$

$$b^2 - 4ac = (A_0k_2 + nk_i)^2 > 0 \tag{21}$$

$$\int\frac{\mathrm{d}p}{A_0k_i + (A_0k_2 - nk_i)P - k_2nP^2} = -\frac{1}{A_0k_2 + nk_i}\ln\frac{k_2nP + nk_i}{k_2(A_0 - nP)} \tag{22}$$

$$\begin{aligned}\int_0^P\frac{\mathrm{d}P}{A_0k_i + (A_0k_2 - nk_i)P - k_2nP^2} &= \frac{1}{A_0k_2 + nk_i}\ln\frac{A_0(k_2P + k_i)}{K_i(A_0 - nP)}\\ &= \int_0 \mathrm{d}t = t\end{aligned} \tag{23}$$

Solving Eq. (23), the function of oxygen uptake P with time t is as follows:

$$P = \frac{A_0}{n}\,\frac{\mathrm{e}^{(A_0k_2+nk_i)t} - 1}{\frac{A_0k_2}{nk_i} + \mathrm{e}^{(A_0k_2+nk_i)t}} \tag{24}$$

As Eq. (24) is too complicated to deal with, let $V = A_0/n$, $K = A_0k_2 + nk_i$, and $L = \mathrm{e}^{Kt_\mathrm{m}} = A_0k_2/nk_i$, so the above equation is given by

$$P = V\frac{\mathrm{e}^{Kt} - 1}{\mathrm{e}^{Kt} + L} \tag{25}$$

This formula can be expressed in another form as illustrated below:

$$P = V\frac{1 - \mathrm{e}^{-Kt}}{1 + L\mathrm{e}^{-Kt}} \tag{26}$$

From the above equation, we know that at $t = \infty$, $\mathrm{e}^{-Kt} = 0$ and $p_\infty = V$, indicating that V is the maximum oxygen uptake in the system (symbolized as V_∞), which is consistent with the definition of $V = A_0/n$.

The second differential equation of P to t is

$$\frac{\partial^2 p}{\partial^2 t} = Vk^2\frac{(L+1)\mathrm{e}^{Kt}(L - \mathrm{e}^{Kt})}{(\mathrm{e}^{Kt} + L)^3} \tag{27}$$

At the time of the maximum rate of oxygen uptake, t_m, $\partial^2P/\partial t^2 = 0$, and L is nonnegative.

Therefore, from Eq. (27) we can obtain the following equation:

$$L = \mathrm{e}^{Kt_\mathrm{m}} \tag{28}$$

The oxygen uptake Eq. (26) can be expressed as the following equation:

$$\begin{aligned} P &= V\frac{1 - \mathrm{e}^{-Kt}}{1 + \mathrm{e}^{Kt_\mathrm{m}}\mathrm{e}^{-Kt}} \\ P &= V\frac{1 - \mathrm{e}^{-Kt}}{1 + \mathrm{e}^{-K(t - t_\mathrm{m})}} \end{aligned} \tag{29}$$

Eq. (29) is the oxygen uptake kinetics equation, where V_∞ is the maximum oxygen uptake, K the combined rate constant and t_m the time at which the oxygen speed is maximized.

$$P_\mathrm{m} = V_\infty\frac{\mathrm{e}^{Kt_\mathrm{m}} - 1}{\mathrm{e}^{Kt_\mathrm{m}} + L} = \frac{V_\infty}{2L}(L - 1) = \frac{V_\infty}{2}\left(1 - \mathrm{e}^{-Kt_\mathrm{m}}\right) \tag{30}$$

Dinoiua et al. [18] realized the importance of the time to reach half of maximum oxidation and used it to make the induction time in their study. From Eq. (29), we know that the maximum oxidizing rate is at the half of maximum oxidation if L is large enough to ignore the difference of L and $(L - 1)$.

$$P_\mathrm{m} = \frac{V_\infty}{2L}(L - 1) \approx \frac{V_\infty}{2} \tag{31}$$

At the inhibition system, L usually is large enough, so that the oxidation rate is a maximum at the time of half of total oxygen uptake.

At t_m, the tangential slope of oxygen uptake curve, $(\partial P/\partial t)_{t_\mathrm{m}}$,

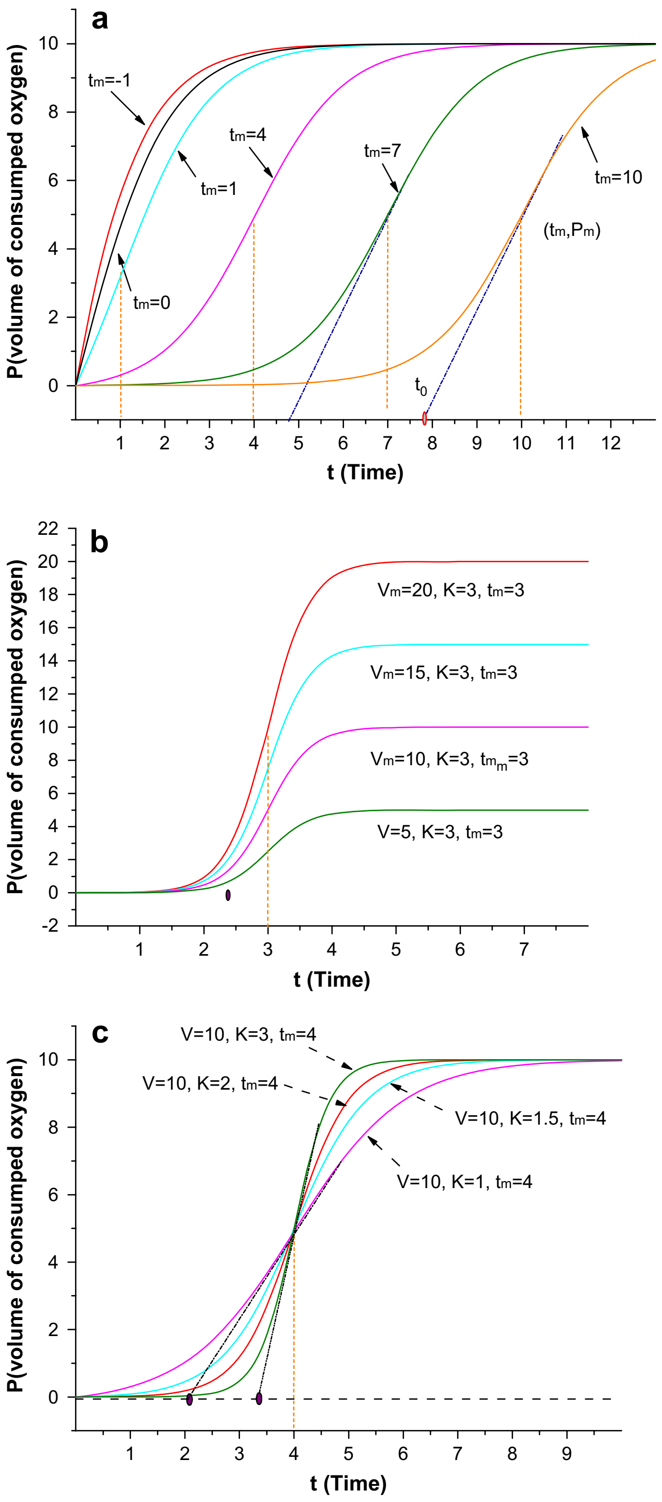

Fig. 2. Constructed example curves of oxygen uptake with varying the parameters of Eq. (29). (a) Varying t_m at constant of K and V_∞. (b) Varying V_∞ at constant of t_m and K. (c) Varying K at constant of t_m and V_∞.

$$\begin{aligned} \left(\frac{\partial P}{\partial t}\right)_{t_\mathrm{m}} &= V_\infty k\frac{\mathrm{e}^{Kt_\mathrm{m}}(L+1)}{(\mathrm{e}^{Kt_\mathrm{m}} + L)^2} = V_\infty K\frac{L(L+1)}{4L^2} = V_\infty K\frac{L+1}{4L} \\ &= \frac{V_\infty K}{4}\left(1 + \mathrm{e}^{-Kt_\mathrm{m}}\right) \end{aligned} \tag{32}$$

From the definition of induction time, t_0, as illustrated in Fig. 2(a), $(P_m/(t_m - t_0)) = V_\infty K(L + 1/4L)$. Thus, the equation about t_0 is as follows:

$$t_0 = \frac{\ln L}{K} - \frac{2(L-1)}{K(L+1)} = t_m - \frac{2(e^{Kt_m}-1)}{K(e^{Kt_m}+1)} \tag{33}$$

If L is large the difference of $(L+1)$ and $(L-1)$ can be ignored.

$$t_0 \approx \frac{\ln L}{K} - \frac{2}{K} = \frac{\ln L - 2}{K} = \frac{Kt_m - 2}{K} = t_m - \frac{2}{K} \tag{34}$$

2.3. Numeric solution methods (fitting of the curves to empirical data, and regression)

For the oxidation of the artificial aging experiment, a series of data about oxygen uptake, p and time t can be obtained (t_i, P_i). The methods by which the parameters V_∞, L and K were obtained from the data set of (t_i, P_i) are described in the appendix in detail.

From Eq. (25), the derivation based Nonlinear Least Squares Fitting method is

$$Q = \sum_{i=1}^{n}\left(P_i - V\frac{e^{Kt_i}-1}{e^{Kt_i}+L}\right)^2 \tag{35}$$

For $\partial Q/\partial V = 0$, Eq. (36) can be obtained.

$$V = \frac{\sum_{i=1}^{n} P_i \frac{e^{Kt_i}-1}{e^{Kt_i}+L}}{\sum_{i=1}^{n} \frac{(e^{Kt_i}-1)^2}{(e^{Kt_i}+L)^2}} \tag{36}$$

For $\partial Q/\partial K = 0$, Eq. (37) can be obtained.

$$V = \frac{\sum_{i=1}^{n} P_i \frac{t_i e^{Kt_i}}{(e^{Kt_i}+L)^2}}{\sum_{i=1}^{n} \frac{t_i e^{Kt_i}(e^{Kt_i}-1)}{(e^{Kt_i}+L)^3}} \tag{37}$$

For $\partial Q/\partial L = 0$, Eq. (38) can be obtained.

$$V = \frac{\sum_{i=1}^{n} P_i \frac{(e^{Kt_i}-1)}{(e^{Kt_i}+L)^2}}{\sum_{i=1}^{n} V \frac{(e^{Kt_i}-1)^2}{(e^{Kt_i}+L)^3}} \tag{38}$$

The parameters of V, K and L can be calculated from Eqs. (36)–(38) based on numerical methods, as illustrated in Appendix 2. The parameter can also easily be calculated by using the advanced fitting tool in the "nonlinear curves fit function" of Origin 7.0 software provided by OriginLab Corporation.

2.4. The constructed sigmoidal curves with different parameters

The effect of V_∞, K, and t_m on the relationship of oxygen uptake with time based on Eq. (29) is clearly illustrated in Fig. 2. The oxygen uptake versus t_m values is plotted in Fig. 2(a), which shows that the induced time increased with increasing t_m, as expressed by Eqs. (33) and (34). No induced time is observed at the condition of $t_m = 0$, indicating that the oxidation rate is initially a maximum and then gradually decreases. This case may be encountered in a practical system in which many radicals have been accumulated before the test or a delayed time counter, just like the movement of the reference frame of coordinates to the right and up along the sigmoidal curves. From Eqs. (17), (24) and (28) $(L = e^{Kt_m} = A_0k_2/nk_i)$, Eq. (39) is

$$L = e^{kt_m} = \frac{A_0 k_p(1-\alpha)}{nk_i\left(m + \sqrt{\frac{k_t}{k_d}}\right)} \tag{39}$$

if $m \ll \sqrt{k_t/k_d}$, Eq. (39) can be expressed as the following equation:

$$L = e^{kt_m} = \frac{A_0}{n}\frac{k_p}{k_i}\sqrt{\frac{k_d}{k_t}}(1-\alpha) \tag{40}$$

And,

$$kt_m = \ln V_\infty + \ln\frac{k_p}{k_i} + \ln\sqrt{\frac{k_d}{k_t}} + \ln(1-\alpha) \tag{41}$$

$$k = A_0k_p(1-\alpha)\sqrt{\frac{k_d}{k_t}} + nk_i \tag{42}$$

The t_m value is expressed in Eq. (43).

$$t_m = \frac{\ln V_\infty + \ln\frac{k_p}{k_i} + \ln\sqrt{\frac{k_d}{k_t}} + \ln(1-\alpha)}{A_0k_p(1-\alpha)\sqrt{\frac{k_d}{k_t}} + nk_i} \tag{43}$$

Examination of Eq. (43) supports the following conclusion: the time to reach the maximum oxygenating speed depends on the ratio of A_0 to n, i.e., V_∞, the ratio of k_p to k_i and the ratio of k_d to k_t. V_∞ is the maximum amount of the oxygen uptake, and hence its large value indicates that more oxygen is needed and more time is needed at the same oxygen speed. The effect of the initiation rate constant k_i on t_m is clearly shown in Eq. (43), t_m is reduced with increasing k_i, otherwise with lower k_i, a longer time is needed to accumulate the free radical and peroxide to accelerate the oxidation speed. However, it is more difficult to understand the effect of parameters k_d, k_p and k_t on t_m because the numerator and denominator both increase or decrease as these parameters are varied. The ratio of k_d/k_t is related to the decomposition of peroxide and the termination of two radicals, in which a higher value indicates a higher value of the free radical in the oxidation process, and, thereby, a faster rate and lower t_m. This can also be proven by analysis of Eq. (43) that although $\ln(\sqrt{k_d/k_t})$ increases with increasing $\sqrt{k_d/k_t}$, the degree of increase has made the logarithm in the numerator, and hence the t_m value, decrease. The effect of k_p on t_m can also be confirmed through the above method that shows the decrease in t_m with increasing k_p, based on Eq. (43).

Fig. 2(a) clearly shows that the shape of the oxygen uptake curves varies according to t_m. The curves for $t_m \leq 1$ are most like Fig. 1(b), and the initial part of the curves like Fig. 1(a) and the whole shape like Fig. 1(c) for $t_m > 1$. This means that Eq. (29) can fit with the three main types of oxygen uptake. The effects of parameters V and K are illustrated by Fig. 2(b) and (c). The maximum amount of oxygen uptake is independent of the parameter V_∞, as seen in Fig. 2(b), and the induced time does not change only according to the parameter V_∞. The parameter K presents the combined oxidation rate constant, which can affect the induced time and the maximum oxidation rate, as illustrated in Fig. 2(c). The shape of oxygen uptake is controlled by the three independent parameters.

3. Comparisons between the proposed model and experimental data for the HMPSA system

In order to check the practicality of the theoretically deduced kinetic equation and comprehend some phenomena in view of the above considerations, the thermo-oxidization equipment was designed for the oxygen uptake test, and the oxygen uptake curves of uninhibited and inhibited systems of the HMPSA ingredients were measured. The experimental

Table 3
Specification of the antioxidants used in the test

Trade name/substance name/CAS no.	Appearance	Melting point (°C)	Structure
Antioxidant 1010/pentaerythritol tetra(3-(3,5-di-*tert*-butyl-4-hydroxyphenyl) propionate)/6683-19-8	White crystal powder	119–123	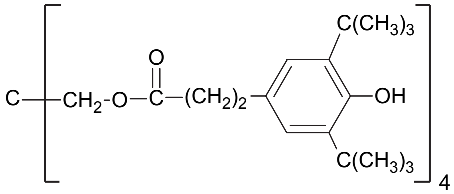
Antioxidant 1076/octadecyl 3-(3,5-di-*tert*-butyl-4-hydroxyphenyl)propionate/2082-79-3	White crystal powder	50–55	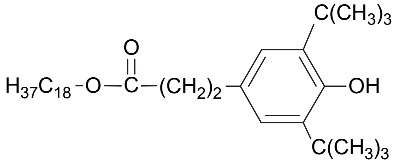
Antioxidant 300/4,4′-thiobis(3-methyl-6-*tert*-butylphenol/96-69-5	White crystal powder	161–164	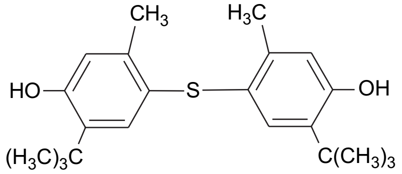
Antioxidant 330/1,3,5-trimethyl-2,4,6-tris(3,5-di-*tert*-butyl-4-hydroxybenzyl) benzene/1709-70-2	White crystal powder	240–250	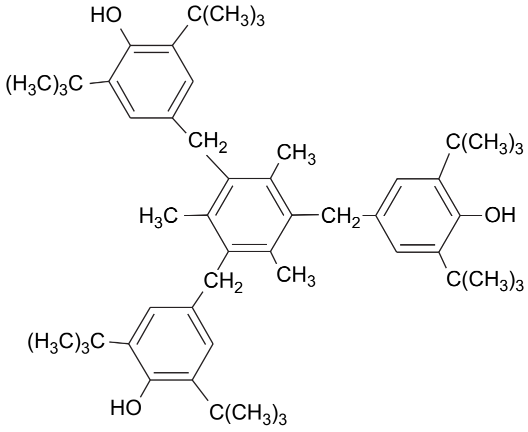
Antioxidant 264/2,6-di-*tert*-butyl-4-methylphenol/128-37-0	White crystal powder	69–71	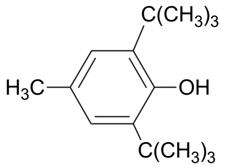

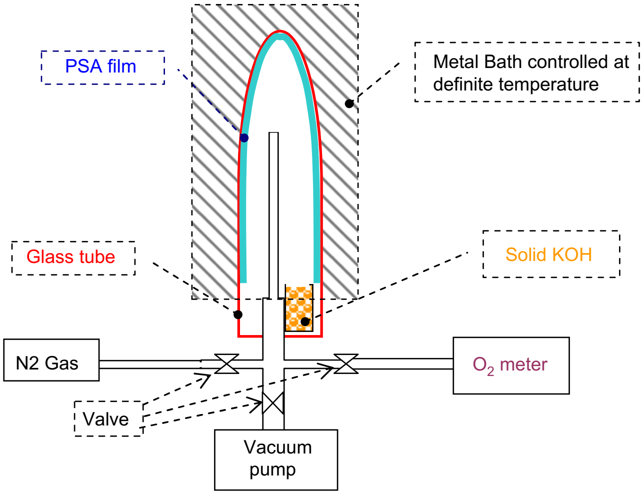

Fig. 3. Scheme of equipment for the oxygen uptake experiment.

data were treated based on the above method. Partial results are presented in this paper.

3.1. Materials

SBS (YH-792), SIS (Kraton D1107) and SEBS (hydrogenated SBS) employed in this study were commercial products supplied by Shell Company, which already contained some antioxidants for total or partial base stabilization. Before preparing the oxidation sample, SBS and SIS were first purified by successive precipitation in methanol from a benzene solution based on the Pecsok method [29] for extracting off the small quantity of initially present antioxidant. After finally being precipitated, the sample was dried in a vacuum drier under 50 °C, and SBS and SIS were resolved in toluene under a nitrogen atmosphere and kept in the dark at 5 °C temperature in a refrigerator. Process oil and tackifier (terpene resin, T-90, soft point: 90 °C, Fengkai Forestry Chemical Factory, China) were directly used with commercial products. The antioxidants employed are listed below. High purity nitrogen was used to prevent oxidation before the metering time of oxidation in the aging process and industrial grade oxygen was used as an oxidizer for the accelerating aging test.

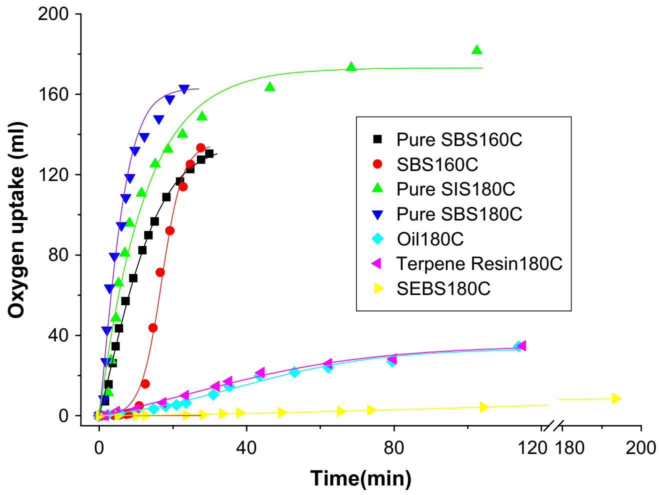

Fig. 4. Oxygen uptake of the HMPSA ingredients (SBS, SIS, terpene resin, oil and SEBS) at 160 and 180 °C in the oxygen atmosphere. Comparison between the model predictions (continuous lines) and the experimental results (points). The model of the fitted function based on Eq. (29) and the related parameters is listed in Table 4.

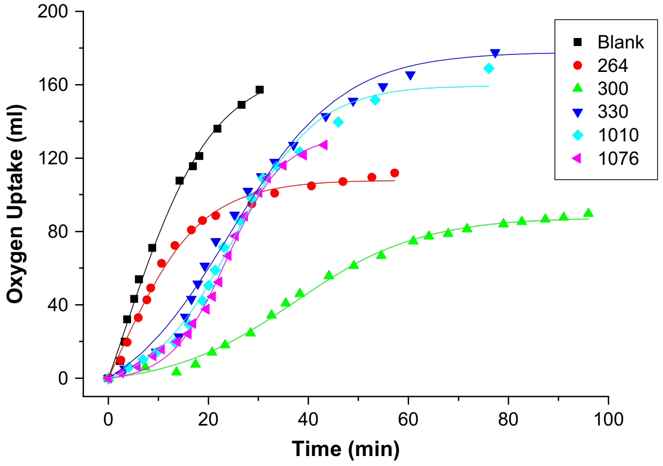

Fig. 5. Oxygen uptakes of the SBS–HMPSA incorporated with various antioxidants at a load of 0.4 wt% at 180 °C in an oxygen atmosphere. The basic formulation of SBS–HMPSA is SBS (YH-792) 100 phr, terpene resin (T-90) 110 phr, and process oil 60 phr, along with 0.4 wt% antioxidant dissolved in toluene at 20% solid content. Comparison between the model predictions (continuous solid lines) and the experimental results (points). The model of the fitted function based on Eq. (29) and the related parameters are listed in Table 6.

The antioxidants employed in this study were commercial products supplied by Beijing Chemical Agent Company with specifications listed in Table 3.

SDS plus antioxidant or PSA sample was prepared in dry toluene under nitrogen atmosphere at room temperature. The

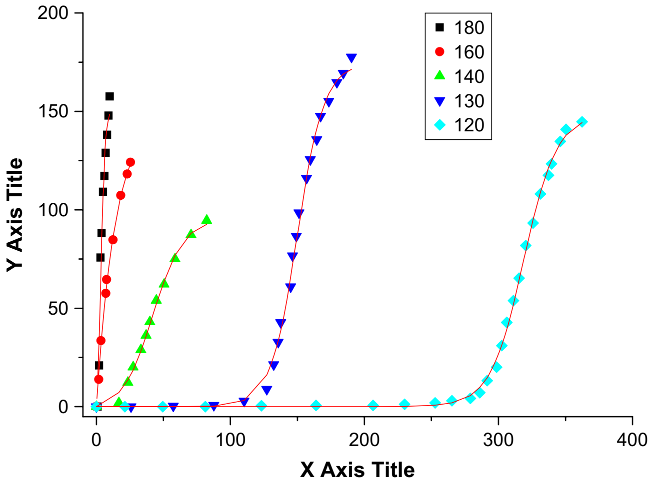

Fig. 6. Oxygen uptakes of the SBS–HMPSA with no antioxidants at different temperatures. The basic formulation of SBS–HMPSA is SBS (YH-792) 100 phr, terpene resin (T-90) 110 phr, and process oil 60 phr, with the mixture dissolved in toluene at 20% solid content. Comparison between the model predictions (continuous solid lines) and the experimental results (points). The model of the fitted function based on Eq. (29) and the related parameters are listed in Table 8.

Table 4
Fitting parameters and related confidence on Eq. (29) of the ingredients for HMPSA

Sample name	The fitting value, errors on parameters and dependence				The correlation of regression curves	
	Parameter name	Value	Error on parameter value	Dependence	Item name	Value
Pure SBS160 °C	V_∞	135.32	3.09607	0.90901	Correlation	0.9989
	K	0.1296	0.01387	0.98161	COD (R^2)	0.9978
	t_m	2.10	1.74576	0.96094	χ^2	5.2325
SBS160 °C	V_∞	128.41	3.27272	0.55834	Correlation	0.9972
	K	0.4225	0.03828	0.35796	COD (R^2)	0.9944
	t_m	16.49	0.26236	0.48403	χ^2	17.7725
Pure SIS180 °C (constraint)	V_∞	166.86	5.02537	0.46641	Correlation	0.9872
	K	0.1338	0.01008	0.46641	COD (R^2)	0.9745
	t_m	0	0		χ^2	96.292
Pure SBS180 °C (constraint)	V_∞	159.27	3.26444	0.62134	Correlation	0.9930
	K	0.2389	0.01122	0.62134	COD (R^2)	0.9861
	t_m	0	0		χ^2	46.6774
Oil 180 °C	V_∞	33.46	1.57872	0.79791	Correlation	0.9932
	K	0.0519	0.00733	0.77632	COD (R^2)	0.9864
	t_m	37.89	2.24795	0.60514	χ^2	1.9040
Terpene resin 180 °C	V_∞	34.97	1.75038	0.86289	Correlation	0.9962
	K	0.0395	0.00803	0.95572	COD (R^2)	0.9925
	t_m	23.761	6.34566	0.89729	χ^2	1.2996
SEBS180 °C	V_∞	9.98	0.51511	0.95605	Correlation	0.9987
	K	0.0214	0.0021	0.89588	COD (R^2)	0.9974
	t_m	107.03	4.20946	0.86022	χ^2	0.0287

films for the accelerating test were cast on the inside glass tube surface, dried under vacuum and any traces of solvent were striped off by nitrogen gas.

3.2. Equipment for oxidation test

The equipment for measuring the oxygen uptake of the SDS and PSA films is illustrated in Fig. 3. Some solid KOH was put in the glass tube, in which the sample coated on the inner surface, to absorb the carbon dioxide and volatile acids produced in the aging process. During the oxidation process, the sample may be deeply oxidized to form the small molecular compounds such as CO_2 or carboxylic acids, which influence the accurate observations of oxygen consumption. The glass tube was first filled with high purity nitrogen by using N_2 gas and a vacuum pump alternately for three times, and then inserted into a hole in an aluminum bath kept at the designed temperature and held for 5 min in order to bring the glass tube to a constant temperature. After nitrogen was replaced with oxygen by changing the valves of the vacuum pump and using oxygen three times for a short interval, the volume of consumed oxygen was recorded.

Table 5
Compound parameters (nk_i, A_0k_2 and k_2/k_1) of HMPSA ingredients

Sample name	nk_i	A_0k_2	k_2/k_1
Pure SBS160 °C	0.056036	0.073564	0.009701
SBS160 °C	0.000398	0.422102	8.263074
Pure SIS180 °C (constraint)	0.0669	0.0669	0.005993
Pure SBS180 °C (constraint)	0.11945	0.11945	0.006279
Oil 180 °C	0.006372	0.045528	0.213555
Terpene resin 180 °C	0.011107	0.028393	0.0731
SEBS180 °C	0.001967	0.019433	0.98991

3.3. Numerical regression methods and conditions

The regression simulation of the experimental data was carried out in the following conditions. The tolerance was set at 1.0×10^{-9}, which is the standard value to judge the iterations performed if the change of the value of the reduced χ^2 between two successive iterations is less than it. The delta was set at 0.05 from a minimum 5×10^{-30} to a maximum 5×10^{30} with no weighting and no constraint conditions for parameter regression programmed unless a special declaration was made. The errors on the parameter values, dependence, correlation coefficient and reduced χ^2 coefficient of determination (R^2) were also calculated.

3.4. Experimental results and discussion

3.4.1. Thermal oxidation behavior of related ingredients and HMPSA

SBS-type PSAs are usually multi-component formulations including SBS or SIS, tackifier and plastic oil. The oxidizing behavior has been observed to differ greatly with different ingredients, which contribute to their different chemical structures. As illustrated in Fig. 4, the oxidation curves of pure SIS (denoted as pure SIS180 °C) and of pure SBS (pure SBS180 °C) at 180 °C were similar and their oxygen uptakes

Table 6
Fitting parameters and related confidence on Eq. (29) of PSA with various antioxidants at 0.4% content

Sample name	The fitting value, errors on parameters and dependence				The correlation of regression curves	
	Parameter name	Value	Error on parameter value	Dependence	Item name	Value
Blank	V_∞	168.7	9.37187	0.94626	Correlation	0.99737
	K	0.11127	0.02273	0.98498	COD (R^2)	0.99475
	t_m	2.97	3.24901	0.95758	χ^2	19.40399
264	V_∞	107.9	2.42618	0.62898	Correlation	0.99684
	K	0.11765	0.02098	0.9602	COD (R^2)	0.9937
	t_m	1.15	4.42353	0.94781	χ^2	9.84553
300	V_∞	87.8	2.39445	0.67368	Correlation	0.99812
	K	0.07996	0.00929	0.57853	COD (R^2)	0.99625
	t_m	37.31	1.23091	0.36836	χ^2	4.35125
330	V_∞	177.9	2.80836	0.67669	Correlation	0.99431
	K	0.08889	0.00573	0.69536	COD (R^2)	0.98866
	t_m	24.24	0.58506	0.50017	χ^2	47.24356
1010	V_∞	159.7	3.32665	0.68885	Correlation	0.99608
	K	0.12014	0.00818	0.47941	COD (R^2)	0.99218
	t_m	25.0	0.48353	0.50587	χ^2	26.06267
1076	V_∞	131.8	4.24395	0.80049	Correlation	0.99791
	K	0.1793	0.01448	0.55067	COD (R^2)	0.99582
	t_m	23.67	0.50584	0.71116	χ^2	9.10583

exceeded 160 ml/g, while those of process oil and tackifier were almost the same at less than 40 ml/g oxygen uptake at the final recording. SEBS (SEBS180 °C) demonstrated very good resistance to thermal oxidation. For the purified SBS sample described in Section 3.1 (pure SBS160 °C) and the original commercial one (SBSC160 °C) at 160 °C, the oxygen uptake curves differed greatly at the initial stage with induced time for inhibited SBS (SBS160 °C), but no induced time was observed for the sample of pure SBS at 160 °C (pure SBS160 °C in Fig. 4). After 20 min, the curve of SBS (SBS160 °C) caught up with that of pure SBS (pure SBS160 °C) with a sharp slope, indicating that the inhibited SBS system showed a faster oxidation speed after induced time than did pure SBS, which was attributed to the acceleration of the oxidized antioxidant product. From the results shown in Fig. 4, it is clear that the oxygen uptake behaviors of the HMPSA materials differed greatly at the maximum amount of oxygen uptake, induction time, maximum oxidizing speed and time dependence, especially for SDS, tackifier and process oils, due to the differences in their chemical structures. The oxidizable group contents $[A]_0$ in SDS were more than those in the tackifier, oil or SEBS. Comparing the same sample at different temperatures, the maximum amount of oxygen and the maximum oxidizing speed increased with increasing temperature, demonstrating the dependence of the oxidizable group contents $[A]_0$ on the test conditions.

Table 7
Compound parameters (nk_i, A_0k_2 and k_2/k_1) of PSA with various antioxidants at 0.4% content

Sample name	nk_i	A_0k_2	k_2/k_1
Blank	0.046524	0.064746	0.008251
264	0.054862	0.062788	0.010605
300	0.003854	0.076106	0.224954
330	0.009235	0.079655	0.048494
1010	0.005675	0.114465	0.126325
1076	0.002535	0.176765	0.529236

The oxygen curves of the SBS-type PSA films with various sterically hindered phenol antioxidants are shown in Fig. 5. The curves of the samples inhibited with antioxidants 330, 1076 and 1010 were similar, indicating that they have similar deduction times and maximum oxygen uptakes, whereas antioxidants 264 and 330 had lower maximum oxygen uptakes. Moreover, antioxidant 264 had little effect on delaying the start of oxidization, in contrast to the uninhibited one, while antioxidant 330 had a stronger inhibition effect for the SBS–PSA system with a long deduction time and low maximum oxygen. Despite being sterically hindered phenols, all these antioxidants had different autoxidation behaviors for SBS-type HMPSA.

The oxygen curves of SBS-type PSA films with no antioxidant at different temperatures are shown in Fig. 6. The induction time strongly depended on the test temperature, especially in the range from 120 to 160 °C. Induction time is generally considered to be the period over which the antioxidant is consumed. However, in the absence of any antioxidant system, it can be considered as the accumulation period of free radicals and peroxide. As the oxidizing rate is related to the number of remaining oxidizable groups and the number of oxidized groups in the system, the maximum rate is usually half of the maximum volume of the oxygen uptake. In other words, the maximum rate usually takes place at the movement when the half of the oxidizable groups has been oxidized (Eq. (31)).

3.4.2. Numeric solution and the prediction model

The experimental data were simulated by Eq. (29) by using the methods described in Section 3.2, and the fitting parameters and the regression conditions are shown in Table 4. Many types of oxygen uptake curves are presented in Fig. 4, all of which can be fitted using the proposed model with good correlation coefficients and with the coefficient of determination over 0.98, as indicated in Table 4.

For the sample of pure SIS and SBS oxidized at 180 °C, the oxygen speed was initially too fast for any induction time to be detected, suggesting that the maximum oxidization time was earlier than the starting record time. This may be explained by the pre-oxidizing of the sample before starting to measure the oxidizing time, during the heating of the glass tube coated with the sample to test the temperature under the nitrogen atmosphere and then transform to oxygen atmosphere, as indicated in Fig. 1. Because pure SBS and SIS are more sensitive to oxidization, these samples at high temperature easily reach the maximum oxidizing speed with only a small peroxide content. As to the regression process of the parameters of the pure SIS180 °C and pure SBS180 °C samples, the constraint condition is $t_m \geq 0$ while the other samples and parameters have no constraints.

The predicted curves of oxygen uptake for each sample are plotted in Fig. 4 in a continuous solid line on the model function which is constructed by the parameters V_∞, K and t_m listed in Table 4 and corresponding to Eq. (29). Each parameter-related property, such as error and dependence, as well as the correlation of the curve with the data, educed the χ^2 coefficient of determination (R^2) is listed in Table 5. All the predicted curves exhibited greater consistency with the experimental data, as demonstrated by the high correlation coefficients and coefficients of determination.

The fitting parameter K for the nonpurified SBS at 160 °C was about 0.4225, which was more than three times that of the purified SBS at 160 °C. From the equation, we know that $K = A_0k_2 + nk_i$, $L = (A_0k_2/nk_i) = e^{Kt_m}$, and the following equation can be obtained.

$$A_0k_2 = nk_i e^{Kt_m} \tag{44}$$

$$K = A_0k_2 + nk_i = nk_i e^{Kt_m} + nk_i = nk_i\left(1 + e^{Kt_m}\right) \tag{45}$$

$$nk_i = \frac{K}{1 + e^{Kt_m}} \tag{46}$$

$$A_0k_2 = nk_i e^{Kt_m} = \frac{K e^{Kt_m}}{1 + e^{Kt_m}} = \frac{K}{1 + e^{-Kt_m}} \tag{47}$$

From Eqs. (46) and (47) and $V_\infty = A_0/n$, we can calculate the A_0k_2, nk_i and k_2/k_i, as shown in Table 5. Therefore, if we know A_0, we can obtain the values of k_2, n, and k_i. Comparing the values of nk_i, A_0k_2 and k_2/k_i of uninhibited SBS (pure SBS160 °C) with those of inhibited SBS (SBS160 °C), the inhibited system has a greater value of k_2/k_i, indicating that the commercial inhibited SBS has a lower initiation rate constant, possibly because the antioxidant takes part in the initial oxidation and makes the apparent initiation rate constants with lower value. Comparing the uninhibited SBS and SIS systems at 180 °C, SBS is somewhat easily oxidized in contrast to SIS because of the higher nk_i, A_0k_2 and k_2/k_i.

The parameters for Fig. 5 were calculated by the same method as mentioned above and are listed in Tables 6 and 7. The correlation data listed in Table 6 and the predicted oxygen uptake curves for each sample plotted in Fig. 4 clearly show that the equation can also be used for the inhibited HMPSA system with good consistency with the experimental data. The V_∞ in Table 5 varied according to the type of antioxidant employed, possibly due to the difference of the oxygen uptake of the antioxidant, or the change of mechanism by the

Table 8
Fitting parameters and related confidence on Eq. (29) of PSA with no antioxidant at different temperatures (120–180 °C)

Sample name	The fitting value, errors on parameters and dependence				The correlation of regression curves	
	Parameter name	Value	Error on parameter value	Dependence	Item name	Value
180 °C	V_∞	151.3	4.12016	0.7682	Correlation	0.9926
	K	0.60931	0.07675	0.83757	COD (R^2)	0.98525
	t_m	3.23	0.18632	0.60559	χ^2	35.82474
160 °C	V_∞	130.5	3.9408	0.79302	Correlation	0.9977
	K	0.13205	0.00809	0.79302	COD (R^2)	0.99541
	t_m	0	0	0	χ^2	10.73327
140 °C	V_∞	95.58	5.01282	0.77416	Correlation	0.9872
	K	0.08763	0.01282	0.53129	COD (R^2)	0.9745
	t_m	42.19	1.6329	0.6605	χ^2	96.292
130 °C	V_∞	174.4	3.30104	0.72453	Correlation	0.99451
	K	0.10022	0.00542	0.46323	COD (R^2)	0.98906
	t_m	145.96	0.63985	0.63372	χ^2	12.926
120 °C	V_∞	148.7	4.32825	0.80428	Correlation	0.99884
	K	0.08071	5.33E−03	0.54814	COD (R^2)	0.99767
	t_m	318.86	1.16689	0.74483	χ^2	0.78951

Table 9
Compound parameters (nk_i, A_0k_2 and k_2/k_1) of PSA with no antioxidant at different temperatures (120–180 °C)

Sample name	nk_i	A_0k_2	k_2/k_1
180 °C	0.074514	0.534796	0.047434
160 °C	0.069508	0.008732	0.000865
140 °C	0.00212	0.08551	0.422235
130 °C	2.98E−08	0.10022	19288.53
120 °C	5.37E−13	0.08071	1.01E+09

antioxidant. The structure of the antioxidant listed in Table 3 provides greater support for the latter reason.

Tables 8 and 9 list the parameters obtained from the data in Fig. 6 using the same methods. The predicted curves are very close to the experimental data with good correlation, as seen in Table 7. The results confirmed that Eq. (29) can be used to simulate the oxygen uptake of the HMPSA system at different temperatures. The t_m value greatly increased with decreasing test temperature, especially over the low temperature range from 160 to 120 °C, which was attributed to the lower initial reaction rate constants as shown in Table 8. In contrast to the variation of the nk_i value with temperature, the value of A_0k_2 changed little, indicating that temperature has little effect on the value of $A_0(k_p(1-\alpha)/(m+\sqrt{k_t/k_d}))$ correspondingly.

4. Conclusion

Although the autoxidation processes of polymers are very complicated and dependent on the kinds and structures of the polymers, the kinetic equation for oxygen uptake was established in a simple form with the parameters of the maximum oxygen uptake, V_∞, the compound oxidizing rate constant, K, and the maximum oxidizing time, t_m. The significance of the parameters in the formula was easy to understand. The methods for obtaining the parameter values were also proposed using iterative computations from the experimental data.

The proposed methods were successfully applied to the HMPSA system, with variations in the ingredients and the formulations with or without an antioxidant, at different temperatures. Despite the oxygen uptake curve types being of a distinct induction period or not, the model produced results consistent with the experimental data over the range of parameter variations, including the final equilibrium stage.

The model was based on the following assumptions: the formation of alkyl free radicals includes the spontaneous reaction of the oxidizable group, reactions of the oxidizable group with peroxide free radicals and alkoxy free radicals have the same rate constant, and the termination rate of the total peroxide free radical equilibrium agreed with that of the decomposition of the peroxide produced in the oxidation. In other words, the oxidizing reactions include the spontaneous oxidation of the substrate and consequent oxidation led by oxidized products. This study has opened many questions such as the dynamics of multi-substrate systems and the method to obtain the parameters of A_0, n, k_i and k_p; their elucidation will require further study.

Acknowledgements

The authors are grateful for the graduate fellowship provided by the Ministry of Education through the Brain Korea 21 project.

Appendix 1. Deductive process to determine the oxygen uptake

$$\int \frac{1}{ax^2+bx+c}\,\mathrm{d}x = -\frac{2}{\sqrt{b^2-4ac}}\operatorname{arctanh}\frac{2ax+b}{\sqrt{b^2-4ac}}$$
$$= \frac{1}{\sqrt{b^2-4ac}}\ln\left|\frac{2ax+b-\sqrt{b^2-4ac}}{2ax+b+\sqrt{b^2-4ac}}\right|$$
$$\left(\text{for } 4ac-b^2<0\right)$$

$$\frac{\mathrm{d}p}{A_0k_1+\left(A_0k_2-nk_1\right)P-k_2nP^2}=\mathrm{d}t$$

$$a=-k_2n; b=(A_0k_2-nk_1); c=A_0k_1$$

$$\begin{aligned}b^2-4ac &= (A_0k_2-nk_1)^2-4(-k_2n)A_0k_1\\ &= (A_0k_2)^2-2A_0k_2nk_1+(nk_1)^2+4k_2nA_0k_1\\ &= (A_0k_2)^2-2A_0k_2nk_1+(nk_1)^2+4A_0k_2nk_1\\ &= (A_0k_2)^2+2A_0k_2nk_1+(nk_1)^2\\ &= (A_0k_2+nk_1)^2\end{aligned}$$

hence, $b^2-4ac>0$

$$b^2-4ac=(A_0k_2+nk_1)^2$$

$$\sqrt{b^2-4ac}=A_0k_2+nk_1$$

$$\begin{aligned}&\int\frac{\mathrm{d}p}{A_0k_1+(A_0k_2-nk_1)P-k_2nP^2}\\ &=\frac{1}{A_0k_2+nk_1}\ln\left|\frac{-2k_2nP+A_0k_2-nk_1-(A_0k_2+nk_1)}{-2k_2nP+A_0k_2-nk_1+(A_0k_2+nk_1)}\right|\\ &=\frac{1}{A_0k_2+nk_1}\ln\left|\frac{-2k_2nP+A_0k_2-nk_1-A_0k_2-nk_1}{-2k_2nP+A_0k_2-nk_1+A_0k_2+nk_1}\right|\\ &=\frac{1}{A_0k_2+nk_1}\ln\left|\frac{-2k_2nP-2nk_1}{-2k_2nP+2A_0k_2}\right|\\ &=\frac{1}{A_0k_2+nk_1}\ln\left|\frac{-2n(k_2P+k_1)}{-2k_2(nP-A_0)}\right|\\ &=\frac{1}{A_0k_2+nk_1}\ln\left|\frac{n(k_2P+k_1)}{k_2(nP-A_0)}\right|\end{aligned}$$

$$(A_0-A=nP, A_0-nP=A>0, |k_2(nP-A_0)|=k_2(A_0-nP))$$
$$=\frac{1}{A_0k_2+nk_1}\ln\frac{k_2nP+nk_1}{k_2(A_0-nP)}$$

$$\int \frac{\mathrm{d}p}{A_0k_1 + (A_0k_2 - nk_1)P - k_2nP^2} = \frac{1}{A_0k_2 + nk_1}\ln\frac{k_2nP + nk_1}{k_2(A_0 - nP)}$$

$$\int_0^p \frac{\mathrm{d}P}{A_0k_1 + (A_0k_2 - nk_1)P - k_2nP^2} = \frac{1}{A_0k_2 + nk_1}\ln\frac{k_2nP + nk_1}{k_2(A_0 - nP)}\bigg|_0^p$$

$$= \frac{1}{A_0k_2 + nk_1}\ln\frac{k_2np + nk_1}{k_2(A_0 - np)} - \frac{1}{A_0k_2 + nk_1}\ln\frac{nk_1}{A_0k_2}$$

$$= \frac{1}{A_0k_2 + nk_1}\left(\ln\frac{k_2np + nk_1}{k_2(A_0 - np)} - \ln\frac{nk_1}{A_0k_2}\right)$$

$$= \frac{1}{A_0k_2 + nk_1}\ln\frac{\dfrac{n(k_2p + k_1)}{k_2(A_0 - np)}}{\dfrac{nk_1}{A_0k_2}}$$

$$= \frac{1}{A_0k_2 + nk_1}\ln\frac{A_0k_2n(k_2p + k_1)}{k_1k_2n(A_0 - np)}$$

$$= \frac{1}{A_0k_2 + nk_1}\ln\frac{A_0(k_2p + k_1)}{k_1(A_0 - np)}$$

$$\int_0^t \mathrm{d}t = t$$

$$\frac{1}{A_0k_2 + nk_1}\ln\frac{A_0(k_2p + k_1)}{k_1(A_0 - np)} = t$$

$$\ln\frac{A_0(k_2p + k_1)}{k_1(A_0 - np)} = (A_0k_2 + nk_1)t$$

$$\frac{A_0(k_2p + k_1)}{k_1(A_0 - np)} = \mathrm{e}^{(A_0k_2 + nk_1)t}$$

$$\frac{k_2p + k_1}{A_0 - np} = \frac{k_1}{A_0}\mathrm{e}^{(A_0k_2 + nk_1)t}$$

$$k_2p + k_1 = (A_0 - np)\frac{k_1}{A_0}\mathrm{e}^{(A_0k_2 + nk_1)t}$$

$$k_2p + k_1 = A_0\frac{k_1}{A_0}\mathrm{e}^{(A_0k_2 + nk_1)t} - np\frac{k_1}{A_0}\mathrm{e}^{(A_0k_2 + nk_1)t}$$

$$k_2p + k_1 = k_1\mathrm{e}^{(A_0k_2 + nk_1)t} - \frac{nk_1p}{A_0}\mathrm{e}^{(A_0k_2 + nk_1)t}$$

$$k_2p + \frac{nk_1p}{A_0}\mathrm{e}^{(A_0k_2 + nk_1)t} = k_1\mathrm{e}^{(A_0k_2 + nk_1)t} - k_1$$

$$p\left(k_2 + \frac{nk_1}{A_0}\mathrm{e}^{(A_0k_2 + nk_1)t}\right) = k_1\left(\mathrm{e}^{(A_0k_2 + nk_1)t} - 1\right)$$

$$p\left(k_2 + \frac{nk_1}{A_0}\mathrm{e}^{(A_0k_2 + nk_1)t}\right) = k_1\left(\mathrm{e}^{(A_0k_2 + nk_1)t} - 1\right)$$

$$p = \frac{k_1\left(\mathrm{e}^{(A_0k_2 + nk_1)t} - 1\right)}{k_2 + \dfrac{nk_1}{A_0}\mathrm{e}^{(A_0k_2 + nk_1)t}}$$

$$= \frac{A_0}{nk_1}\,\frac{k_1\left(\mathrm{e}^{(A_0k_2 + nk_1)t} - 1\right)}{\left(k_2 + \dfrac{nk_1}{A_0}\mathrm{e}^{(A_0k_2 + nk_1)t}\right)\dfrac{A_0}{nk_1}}$$

$$= \frac{A_0}{nk_1}\,\frac{k_1\left(\mathrm{e}^{(A_0k_2 + nk_1)t} - 1\right)}{\dfrac{A_0k_2}{nk_1} + \mathrm{e}^{(A_0k_2 + nk_1)t}}$$

$$P = \frac{A_0}{n}\,\frac{\mathrm{e}^{(A_0k_2 + nk_1)t} - 1}{\dfrac{A_0k_2}{nk_1} + \mathrm{e}^{(A_0k_2 + nk_1)t}}$$

Let $k = A_0k_2 + nk_1$, $L = A_0k_2/nk_1$, $V = A_0/n$

$$p = V\frac{\mathrm{e}^{kt} - 1}{\mathrm{e}^{kt} + L}$$

$$p = V\frac{1 - \mathrm{e}^{-kt}}{1 + L\mathrm{e}^{-kt}}$$

$$p = V\frac{1 - \mathrm{e}^{-kt}}{1 + L\mathrm{e}^{-kt}} = V\frac{\mathrm{e}^{kt} - 1}{\mathrm{e}^{kt} + L}$$

$$\frac{\partial p}{\partial t} = V\left(\frac{k\mathrm{e}^{kt}}{\mathrm{e}^{kt} + L} - \frac{k(\mathrm{e}^{kt} - 1)\mathrm{e}^{kt}}{(\mathrm{e}^{kt} + L)^2}\right)$$

$$= V\left(\frac{k\mathrm{e}^{kt}(\mathrm{e}^{kt} + L)}{(\mathrm{e}^{kt} + L)^2} - \frac{k(\mathrm{e}^{kt} - 1)\mathrm{e}^{kt}}{(\mathrm{e}^{kt} + L)^2}\right)$$

$$= Vk\frac{\mathrm{e}^{2kt} + L\mathrm{e}^{kt} - (\mathrm{e}^{2kt} - \mathrm{e}^{kt})}{(\mathrm{e}^{kt} + L)^2}$$

$$= Vk\frac{\mathrm{e}^{2kt} + L\mathrm{e}^{kt} - \mathrm{e}^{2kt} + \mathrm{e}^{kt}}{(\mathrm{e}^{kt} + L)^2}$$

$$= Vk\frac{L\mathrm{e}^{kt} + \mathrm{e}^{kt}}{(\mathrm{e}^{kt} + L)^2}$$

$$= Vk\frac{\mathrm{e}^{kt}(L + 1)}{(\mathrm{e}^{kt} + L)^2}$$

$$\frac{\partial p}{\partial t} = Vk\frac{\mathrm{e}^{kt}(L + 1)}{(\mathrm{e}^{kt} + L)^2}$$

$$\frac{\partial^2 p}{\partial^2 t} = Vk\left(\frac{k(L + 1)\mathrm{e}^{kt}}{(\mathrm{e}^{kt} + L)^2} - \frac{\mathrm{e}^{kt}(L + 1)\,\mathrm{e}^{kt}2k}{(\mathrm{e}^{kt} + L)^3}\right)$$

$$\frac{\partial^2 p}{\partial^2 t} = Vk\left(\frac{k(L + 1)\mathrm{e}^{kt}(\mathrm{e}^{kt} + L)}{(\mathrm{e}^{kt} + L)^3} - \frac{2k(L + 1)\mathrm{e}^{kt}\,\mathrm{e}^{kt}}{(\mathrm{e}^{kt} + L)^3}\right)$$

$$\frac{\partial^2 p}{\partial^2 t} = Vk\frac{k(L + 1)\mathrm{e}^{kt}(\mathrm{e}^{kt} + L - 2\mathrm{e}^{kt})}{(\mathrm{e}^{kt} + L)^3}$$

$$\frac{\partial^2 p}{\partial^2 t} = Vk^2\frac{(L + 1)\mathrm{e}^{kt}(L - \mathrm{e}^{kt})}{(\mathrm{e}^{kt} + L)^3}$$

Suppose the time at maximum oxidizing rate is t_m, $\partial^2 p/\partial^2 t = 0$

$$L = \mathrm{e}^{kt_\mathrm{m}}$$

Suppose the value of P at t_m is P_m,

$$p = V\frac{1 - \mathrm{e}^{-kt}}{1 + L\mathrm{e}^{-kt}} = V\frac{\mathrm{e}^{kt} - 1}{\mathrm{e}^{kt} + L},$$

hence,

$$p_{\mathrm{m}} = V\frac{\mathrm{e}^{kt_{\mathrm{m}}}-1}{\mathrm{e}^{kt_{\mathrm{m}}}+L} = \frac{V}{2L}(L-1)$$

The slope of p at t_{m} is

$$\frac{\partial p}{\partial t} = Vk\frac{\mathrm{e}^{kt}(L+1)}{(\mathrm{e}^{kt}+L)^2} = Vk\frac{\mathrm{e}^{kt_{\mathrm{m}}}(L+1)}{(\mathrm{e}^{kt_{\mathrm{m}}}+L)^2} = Vk\frac{L(L+1)}{4L^2}$$

$$= Vk\frac{L(L+1)}{(L+L)^2}$$

$$\frac{\partial p}{\partial t} = Vk\frac{L(L+1)}{4L^2}$$

Suppose t_0 is induction time, from the definition of induction time,

$$\frac{p_{\mathrm{m}}}{t_{\mathrm{m}}-t_i} = Vk\frac{L+1}{4L}$$

$$(t_{\mathrm{m}}-t_i) = \frac{4Lp_{\mathrm{m}}}{Vk(L+1)}$$

$$t_i = t_{\mathrm{m}} - \frac{4Lp_{\mathrm{m}}}{Vk(L+1)}$$

From $L = \mathrm{e}^{Kt_{\mathrm{m}}}$, t_{m} is

$$t_{\mathrm{m}} = \frac{\ln L}{k}$$

from the equation of p_{m}

$$p_{\mathrm{m}} = \frac{V}{2L}(L-1)$$

t_{i} is

$$t_i = \frac{\ln L}{k} - \frac{4L}{Vk(L+1)}\frac{V}{2L}(L-1)$$

$$= \frac{\ln L}{k} - \frac{2(L-1)}{k(L+1)}$$

t_{i} is the function of L and k_0.

Appendix 2. Deductive process to determine the solution equation of oxygen uptake

$$p = V\frac{1-\mathrm{e}^{-kt}}{1+L\mathrm{e}^{-kt}}$$

$$Q = \sum_{i=1}^{n}\left(P_i - V\frac{\mathrm{e}^{kt_i}-1}{\mathrm{e}^{kt_i}+L}\right)^2$$

$$\frac{\partial Q}{\partial V} = 0$$

$$\frac{\partial Q}{\partial V} = \sum_{i=1}^{n} 2\left(P_i - V\frac{\mathrm{e}^{kt_i}-1}{\mathrm{e}^{kt_i}+L}\right)\left(-\frac{\mathrm{e}^{kt_i}-1}{\mathrm{e}^{kt_i}+L}\right)$$

$$\frac{\partial Q}{\partial V} = -\sum_{i=1}^{n} 2\left(P_i - V\frac{\mathrm{e}^{kt_i}-1}{\mathrm{e}^{kt_i}+L}\right)\frac{\mathrm{e}^{kt_i}-1}{\mathrm{e}^{kt_i}+L}$$

$$\frac{\partial Q}{\partial V} = -\sum_{i=1}^{n} 2\left(P_i\frac{\mathrm{e}^{kt_i}-1}{\mathrm{e}^{kt_i}+L} - V\frac{(\mathrm{e}^{kt_i}-1)^2}{(\mathrm{e}^{kt_i}+L)^2}\right)$$

$$= -2\left(\sum_{i=1}^{n} P_i\frac{\mathrm{e}^{kt_i}-1}{\mathrm{e}^{kt_i}+L}\right) - V\left(\sum_{i=1}^{n}\frac{(\mathrm{e}^{kt_i}-1)^2}{(\mathrm{e}^{kt_i}+L)^2}\right)$$

$$\sum_{i=1}^{n} P_i\frac{\mathrm{e}^{kt_i}-1}{\mathrm{e}^{kt_i}+L} - V\left(\sum_{i=1}^{n}\frac{(\mathrm{e}^{kt_i}-1)^2}{(\mathrm{e}^{kt_i}+L)^2}\right) = 0$$

$$V = \frac{\sum_{i=1}^{n} P_i\frac{\mathrm{e}^{kt_i}-1}{\mathrm{e}^{kt_i}+L}}{\sum_{i=1}^{n}\frac{(\mathrm{e}^{kt_i}-1)^2}{(\mathrm{e}^{kt_i}+L)^2}}$$

$$\frac{\partial Q}{\partial k} = 0$$

$$Q = \sum_{i=1}^{n}\left(P_i - V\frac{\mathrm{e}^{kt_i}-1}{\mathrm{e}^{kt_i}+L}\right)^2$$

$$\frac{\partial Q}{\partial k} = \sum_{i=1}^{n} 2\left(P_i - V\frac{\mathrm{e}^{kt_i}-1}{\mathrm{e}^{kt_i}+L}\right)\left(-V\left(\frac{t_i\mathrm{e}^{kt_i}}{\mathrm{e}^{kt_i}+L} - \frac{t_i\mathrm{e}^{kt_i}(\mathrm{e}^{kt_i}-1)}{(\mathrm{e}^{kt_i}+L)^2}\right)\right)$$

$$\frac{\partial Q}{\partial k} = -\sum_{i=1}^{n} 2V\left(P_i - V\frac{\mathrm{e}^{kt_i}-1}{\mathrm{e}^{kt_i}+L}\right)\left(\frac{t_i\mathrm{e}^{kt_i}}{\mathrm{e}^{kt_i}+L} - \frac{t_i\mathrm{e}^{kt_i}(\mathrm{e}^{kt_i}-1)}{(\mathrm{e}^{kt_i}+L)^2}\right)$$

$$\frac{\partial Q}{\partial k} = -\sum_{i=1}^{n} 2V\left(P_i - V\frac{\mathrm{e}^{kt_i}-1}{\mathrm{e}^{kt_i}+L}\right) \times \left(\frac{t_i\mathrm{e}^{kt_i}(\mathrm{e}^{kt_i}+L)}{(\mathrm{e}^{kt_i}+L)^2} - \frac{t_i\mathrm{e}^{kt_i}(\mathrm{e}^{kt_i}-1)}{(\mathrm{e}^{kt_i}+L)^2}\right)$$

$$\frac{\partial Q}{\partial k} = -\sum_{i=1}^{n} 2V\left(P_i - V\frac{\mathrm{e}^{kt_i}-1}{\mathrm{e}^{kt_i}+L}\right)\left(\frac{t_i\mathrm{e}^{kt_i}(\mathrm{e}^{kt_i}+L-\mathrm{e}^{kt_i}+1)}{(\mathrm{e}^{kt_i}+L)^2}\right)$$

$$\frac{\partial Q}{\partial k} = -\sum_{i=1}^{n} 2V\left(P_i - V\frac{\mathrm{e}^{kt_i}-1}{\mathrm{e}^{kt_i}+L}\right)\left(\frac{t_i\mathrm{e}^{kt_i}(L+1)}{(\mathrm{e}^{kt_i}+L)^2}\right)$$

$$\frac{\partial Q}{\partial k} = -\sum_{i=1}^{n} 2V(L+1)\left(P_i\frac{t_i\mathrm{e}^{kt_i}}{(\mathrm{e}^{kt_i}+L)^2} - V\frac{t_i\mathrm{e}^{kt_i}(\mathrm{e}^{kt_i}-1)}{(\mathrm{e}^{kt_i}+L)^3}\right)$$

$$\frac{\partial Q}{\partial k} = -2V(L+1)\left(\sum_{i=1}^{n} P_i \frac{t_i \mathrm{e}^{kt_i}}{\left(\mathrm{e}^{kt_i}+L\right)^2} - V\sum_{i=1}^{n} \frac{t_i \mathrm{e}^{kt_i}\left(\mathrm{e}^{kt_i}-1\right)}{\left(\mathrm{e}^{kt_i}+L\right)^3}\right)$$

$$\frac{\partial Q}{\partial k} = 0$$

$$\sum_{i=1}^{n} P_i \frac{t_i \mathrm{e}^{kt_i}}{\left(\mathrm{e}^{kt_i}+L\right)^2} - V\sum_{i=1}^{n} \frac{t_i \mathrm{e}^{kt_i}\left(\mathrm{e}^{kt_i}-1\right)}{\left(\mathrm{e}^{kt_i}+L\right)^3} = 0$$

$$V = \frac{\sum_{i=1}^{n} P_i \frac{t_i \mathrm{e}^{kt_i}}{\left(\mathrm{e}^{kt_i}+L\right)^2}}{\sum_{i=1}^{n} \frac{t_i \mathrm{e}^{kt_i}\left(\mathrm{e}^{kt_i}-1\right)}{\left(\mathrm{e}^{kt_i}+L\right)^3}}$$

$$\frac{\partial Q}{\partial L} = 0$$

$$Q = \sum_{i=1}^{n}\left(P_i - V\frac{\mathrm{e}^{kt_i}-1}{\mathrm{e}^{kt_i}+L}\right)^2$$

$$\frac{\partial Q}{\partial L} = \sum_{i=1}^{n} 2\left(P_i - V\frac{\mathrm{e}^{kt_i}-1}{\mathrm{e}^{kt_i}+L}\right)\left(-V\frac{\left(\mathrm{e}^{kt_i}-1\right)}{\left(\mathrm{e}^{kt_i}+L\right)^2}\right)$$

$$\frac{\partial Q}{\partial L} = -\sum_{i=1}^{n} 2V\left(P_i - V\frac{\mathrm{e}^{kt_i}-1}{\mathrm{e}^{kt_i}+L}\right)\left(\frac{\left(\mathrm{e}^{kt_i}-1\right)}{\left(\mathrm{e}^{kt_i}+L\right)^2}\right)$$

$$\frac{\partial Q}{\partial L} = -\sum_{i=1}^{n} 2V\left(P_i\frac{\left(\mathrm{e}^{kt_i}-1\right)}{\left(\mathrm{e}^{kt_i}+L\right)^2} - V\frac{\left(\mathrm{e}^{kt_i}-1\right)^2}{\left(\mathrm{e}^{kt_i}+L\right)^3}\right)$$

$$V = \frac{\sum_{i=1}^{n} P_i \frac{\left(e^{kt_i}-1\right)}{\left(\mathrm{e}^{kt_i}+L\right)^2}}{\sum_{i=1}^{n} V\frac{\left(\mathrm{e}^{kt_i}-1\right)^2}{\left(\mathrm{e}^{kt_i}+L\right)^3}}$$

References

[1] Aggarwal SL. Structure and properties of block polymers and multiphase polymer systems: an overview of present status and future potential. Polymer 1976;17:938.

[2] Harlan JT, Petershagan LA. In: Skeist I, editor. Handbook of adhesives. 2nd ed. New York: Van Nostrdnd-Reinhold; 1977 [chapter 19].

[3] Kubo J, Onzuka H, Akiba M. Inhibition of degradation in styrene-based thermoplastic elastomers by hydrogen-donating hydrocarbons. Polym Degrad Stab 1994;45:27.

[4] Wang SM, Chang JR, Tsiang RC. Infrared studies of thermal oxidative degradation of polystyrene-*block*-polybutadiene-*block*-polystyrene thermoplastic elastomers. Polym Degrad Stab 1996;52:51.

[5] Allen NS, Barcelona A, Edge M, Wilkinson A, Merchan CG, Quiteria VRS. Aspects of the thermal and photostabilisation of high styrene–butadiene copolymer (SBC). Polym Degrad Stab 2006;91:1395.

[6] Susmita B, Anil KB, Avasthi BN. Degradation of hydrogenated nitrile rubber. Polym Degrad Stab 1991;31:71.

[7] Gugumus F. Aspects of the stabilization mechanisms of phenolic antioxidants in polyolefins. Angew Makromol Chem 1985;137:189.

[8] Chang DM. Methods for study of thermal aging and stabilization of grafted acrylonitrile–butadiene–styrene (ABS) terpolymers. Polym Eng Sci 1982;22:376.

[9] Emanue NM. Thermo-oxidative ageing of polymers. Polym Sci USSR 1985;27:1505.

[10] Kuz'minskii AS. Some urgent problems in the ageing and stabilization of elastomers – review. Polym Sci USSR 1977;19:2509.

[11] Emanue NM. Some problems of chemical physics of ageing and stabilization of polymers. Polym Sci USSR 1979;21:2900.

[12] Va'vra J. Physics and chemistry of aging – early developments. Nucl Instrum Methods A 2003;515:1.

[13] Traian Z, Maria G, Ion M. Effects of some antioxidants on the stability of ethylene–propylene elastomers. Polym Degrad Stab 1995;48:151.

[14] Belyakov VA, Lauterbach G, Pritzkow W, Voerckel V. Kinetics and regioselectivity of the autoxidation of alkylaromatic hydrocarbons. J Prakt Chem 1992;334:373.

[15] Daniel JH, Julian FJ, Yates WR. Aging of pressure-sensitive adhesives I: stability of styrene–isoprene–styrene block copolymer films at 95 °C. Polym Eng Sci 1982;22:865.

[16] Daniel JH, Yates WR, Julian FJ. Aging of pressure-sensitive adhesives III: studies of surface oxidation with multidetector size exclusion chromatography. J Appl Polym Sci 1986;31:1393.

[17] Reich L, Jadrnicek BR, Stivala SS. Kinetics of thermal oxidation of polyolefins – a review. Polym Eng Sci 1971;11:265.

[18] Dinoiua V, Gorghiub LM, Jipab S, Zaharescuc T, Setnescub R, Dumitrescub C. Kinetic study on thermal degradation of low-density polyethylene stabilized with chalcone derivatives. Polym Degrad Stab 2004;85:615.

[19] Gugumus F. Critical antioxidant concentrations in polymer oxidation – I. Fundamental aspects. Polym Degrad Stab 1998;60:85.

[20] Gugumus F. Critical antioxidant concentrations in polymer oxidation – II. Experimental 'proofs'. Polym Degrad Stab 1998;60:99.

[21] Gugumus F. Critical antioxidant concentrations in polymer oxidation – III. Application to lifetime prediction. Polym Degrad Stab 1998; 60:119.

[22] Zabarnick S. Pseudo-detailed chemical kinetic modeling of antioxidant chemistry for jet fuel applications. Energy Fuels 1998;12:547–53.

[23] Kuprowicza NJ, Ervinb JS, Zabarnickb S. Modeling the liquid-phase oxidation of hydrocarbons over a range of temperatures and dissolved oxygen concentrations with pseudo-detailed chemical kinetics. Fuel 2004;83:1795.

[24] Bhattacharya A. Kinetic modeling of liquid phase autoxidation of cumene. Chem Eng J 2007; doi:10.1016/j.cej.2007.04.043.

[25] Colin X, Audouin L, Verdu J. Kinetic modelling of the thermal oxidation of polyisoprene elastomers. Part 1: unvulcanized unstabilized polyisoprene. Polym Degrad Stab 2007;92:886.

[26] Colin X, Audouin L, Verdu J, Huy ML. Kinetic modelling of the thermal oxidation of polyisoprene elastomers. Part 2: effect of sulfur vulcanization on mass changes and thickness distribution of oxidation products during thermal oxidation. Polym Degrad Stab 2007;92:898.

[27] Benson SW. Kinetics of pyrolysis of alkyl hydroperoxides and their O–O bond dissociation energies. J Chem Phys 1964;40:1007.

[28] Hiatt R, Irwin KC. Homolytic decompositions of hydroperoxides. V. Thermal decompositions. J Org Chem 1968;33:1436.

[29] Pecsok RL, Shelton JR, Koenig JL. Fourier transform infrared studies of inhibited autoxidation in *cis*-1,4-polybutadiene. Polym Degrad Stab 1981;3:61.